Simulation of a Rectifier Malfunction on a Offshore Wind System with HVDC Transmission

M. Seixas, R. Melício and V.M.F. Mendes
IDMEC/LAETA-Instituto Superior Técnico
Universidade de Lisboa and Universidade de Évora
Lisbon and Évora, Portugal
ruimelicio@gmail.com

V.M.F. Mendes and C. Couto, *Senior Member, IEEE*
Instituto Superior de Engenharia de Lisboa
Centro Algoritmi, University of Minho
Lisbon and Guimarães, Portugal

Abstract— A new integrated mathematical model for the simulation of an offshore wind system having a rectifier input voltage malfunction at one phase is presented in this paper. The mathematical model considers an offshore variable-speed wind turbine on a floating platform, equipped with a permanent magnet synchronous generator using full-power three-level converter to inject energy into the electric network, through a high voltage direct current transmission submarine cable. The model for the drive train is a discrete three mass, incorporating the dynamic of the moving surface. A case study is presented to access conclusion about the malfunction.

Keywords—Offshore Wind System; HVDC; three-level converter; rectifier malfunction; simulation.

I. INTRODUCTION

Over the last decades, non-renewable energy sources like oil, coal, nuclear and natural gas have been used as the main source of energy conversion into electric energy [1]. However, disadvantageous circumstances are pointed out in the use of these sources, for instances: for fossil-fuel, the harmful on the environment and the cost subject to market instability and tending to increase in the long run. Forecasts for non-nuclear and non-renewable energy sources are in support of an envisaged scarcity pointing to the exhaustion on those sources in less than a century [2].

Exploitation on renewable energy sources have emerged by support of country polices or by more in-depth protocols such as the Kyoto Protocol as a response to harmful [3] on the environment, instability and increasing fuel costs.

Within the renewable energy sources the wind energy source is experiencing a greater development [4]. This development has achieved such a level that there is an increasing difficulty in new deployment, i.e., a difficulty to find new appropriate places for onshore wind farms. Particularly, a considerable exhaustion on convenient places is reported on Europe [5]. Thus, there is a large interest in the development of offshore wind turbine deployment, having the benefit of available vast sea areas, having more favorable wind conditions, than those on land, because of the non

existence of obstacles [6]. Also, higher and less variation of wind speed values support offshore wind turbine deployment.

Deployment of offshore wind turbines have a less concern with visual and noise impact, allowing the use of wind turbines with larger rotors, allowing a higher value for the installed power [7]. The increase on size of the wind turbines implies that the blades are larger, more flexible and tend to bend. Therefore, the model for the drive train has to capture this fact and this paper proposes a three mass (TM) model taking into account the concern with the dynamic of the blades, the structure and the moving floating platform. Deployment of offshore wind turbines have a power transmission technology depending on the distance from the floating platform to onshore: for distances less than 60 km is proposed to use high-voltage ac (HVAC); for longer distances is proposed high voltage dc (HVDC) [8]. Offshore wind system (offshore wind system) model use classical proportional integral (PI) controllers in order to obtain the reference currents. Also, pulse width modulation (PWM) by space vector modulation (SVM) associated with sliding mode (SM) is used for triggering insulated gate bipolar transistors (IGBTs) in the converter.

The rest of the paper is organized as followed: Section II presents the mechanical and the electric modeling, taking in consideration the dynamic associated with the action excited by the wind on all physical structure on a TM drive train, the converter, the submarine cable HVDC and the electric network. Section III presents the control strategy. Section IV presents the case study dealing with a rectifier input voltage malfunction simulation, using the Matlab/Simulink language. Section V presents concluding remarks.

II. MODELING

The offshore wind system apart from the wind turbine has a rectifier linking a permanent magnet synchronous generator (PMSG) to a first set of two capacity banks. A HVDC transmission submarine cable links the first set of two capacity banks to a second one, connecting to an inverter in order to inject the energy into an electric network through a second order filter to reduce the higher harmonics content in the electric current.

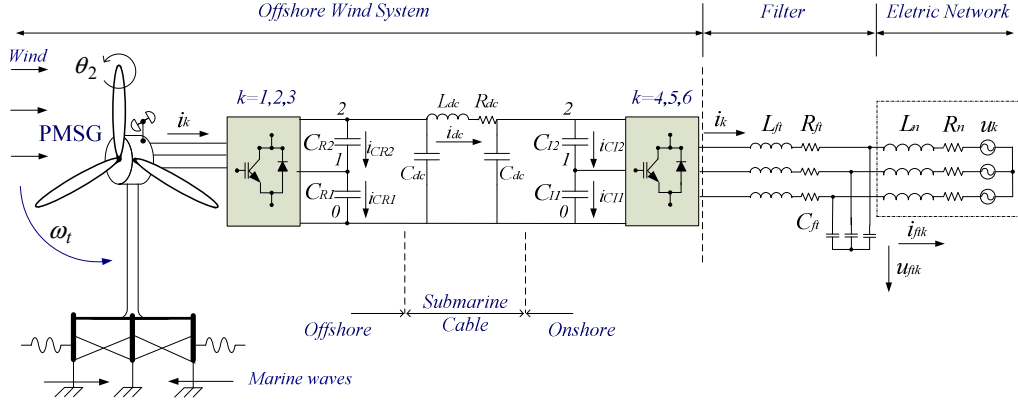The offshore wind system is shown in Fig. 1.

Fig. 1. Offshore Wind System with three-level converter, HVDC.

A. Wind Speed

Although the wind speed has intermittence and variability which can be characterized by stochastic modeling, for the assessment in this paper is possible a deterministic modeling of the wind speed as a sum of harmonics ranging 0.1–10 Hz [9] given by

$$u(t) = u_o[1 + \sum_k A_k \sin(\omega_k t)] \tag{1}$$

where u is the wind speed with perturbation, u_o is the average wind speed, A_k is the magnitude of the k eigenswing, ω_k is the eigenfrequency of the k eigenswing.

B. Turbine and Drive Train

The energy captured from the kinetic energy in the wind is at a rate set by the turbine mechanical power given by

$$P_b = 1/2 \, \phi \, S \, u^3 \, C_p \tag{2}$$

where P_b is the turbine mechanical power, ϕ is the air density, S is the area covered by the turbine blades, C_p is the power coefficient. The power coefficient is given by a function of the rotor blades pitch angle θ and of the tip speed ratio (tsr) λ, which is the ratio between blade tip speed and wind speed. Although, the theory for computing for the power coefficient requires knowledge of blade element theory and the geometry of the blade, for simulation purposes is admissible to use an alternative given by an empirical approximation, for instance, as the one reported in [10]. The approximation consider in this paper assumes a power coefficient given by

$$C_p = 0.73 \, \lambda_k \, e^{-18.4 \, \delta} \tag{3}$$

where λ_k and δ are respectively given by

$$\lambda_k = 151 \delta - 0.58\theta - 0.002\theta^{2.14} - 13.2 \tag{4}$$

$$\delta = 1/(\lambda - 0.02\theta) - 0.003/(\theta^3 + 1) \tag{5}$$

A graphical representation for the C_p in (3) as a function of λ and parameterized in function θ is shown in Fig. 2.
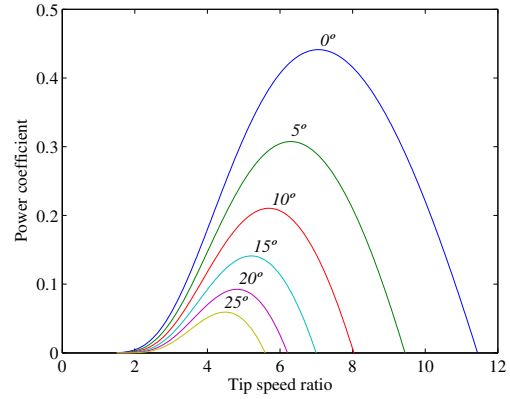
Fig. 2. Power coefficient as a function of λ and parameterized in function θ.

The maximum C_p is obtain with a null θ and is given by

$$C_{p\,\max} = 0.4412 \tag{6}$$

$$\lambda_{opt} = 7.057 \tag{7}$$

where (7) is the value for the tsr at the maximum C_p.

The mass discretization for the drive train and the respective acting torques are shown in Fig. 3.
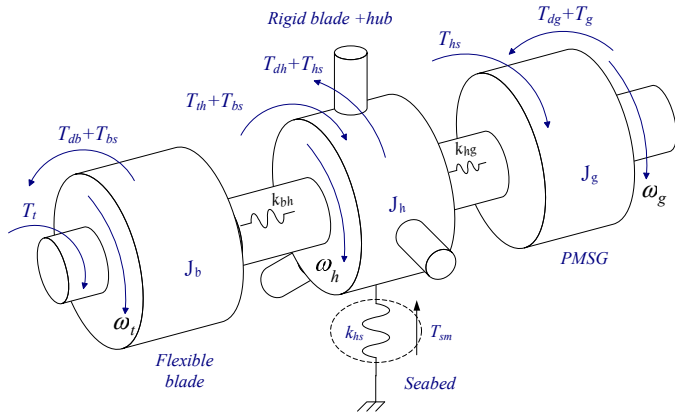

Fig. 3. Three Mass drive train.

The first mass concentrates the inertia of the blades flexible part; the second mass concentrates the blades rigid part, hub, tower and platform, discarding the movement between the different elements, but including the floating motion influence as an whole on the second mass; the third mass concentrates the inertia of the generator. The torsional version of the second law of Newton allows stating the equations for the drive train motion given by

$$\frac{d\omega_t}{dt} = \frac{1}{J_b}(T_t - T_{db} - T_{bs}) \tag{8}$$

$$\frac{d\omega_h}{dt} = \frac{1}{J_h}(T_{th} + T_{bs} + T_{sm} - T_{dh} - T_{hs}) \tag{9}$$

$$\frac{d\omega_g}{dt} = \frac{1}{J_g}(T_{hs} - T_{dg} - T_g) \tag{10}$$

where ω_t is the rotor angular speed at flexible blades part, J_b is the moment of the inertia of the rotating parts at the flexible blades part, T_t is the mechanical torque, T_{db} is the resistant bearing torque due to the damping at the flexible blades part, T_{bs} is the resistant shaft stiffness torque between the flexible blades part and hub, ω_h is the rotor angular speed, at the hub plus rigid blades part, J_h is the moment of the inertia of the rotating parts of the hub plus rigid blades part, T_{th} is the mechanical torque of the rigid blades part, T_{sm} is the tower and platform stiffness torque due to floating surface motion, T_{dh} is the hub bearing resistant torque, T_{hs} is the shaft stiffness torque, between hub and generator, ω_g is the rotor angular speed at the generator, J_g is the moment of inertia of

the rotating parts of the generator, T_{dg} is the generator bearing resistant torque, T_g is the electric torque.

The wind turbine power P_b over the rotor, considering the flexible and rigid part of the blades in the TM drive train without dynamic influences is given by

$$P_b = P_{fb} + P_{rb} \tag{11}$$

where

$$P_{fb} = 1/2 \, \phi \pi (R^2 - r^2) u^3 \, C_p \tag{12}$$

$$P_{rb} = 1/2 \, \phi \pi r^2 \, u^3 \, C_p \tag{13}$$

where P_{fb} is the mechanical power of the blades flexible part, P_{rb} is the mechanical power of the blades rigid part, R is the radius of the area covered by the blades, r is the radius of the area covered by the rigid blades part.

C. PMSG

The PMSG modeling can be retrieved in diverse text [11]. This modeling is subjected to the constraint of having a null reference stator direct component current, $i_{sd}^* = 0$, imposed to avoid demagnetization of permanent magnet [12].

D. Three-Level Converter

Two three-level converters are modeled respectively: a rectifier and an inverter. Both converters has twelve unidirectional commanded IGBTs in order to implement the respectively functionality [13].

The group of four IGBTs associated in the same phase of a converter is said to be the converter's k leg. A switching variable n_k with $n_k \in \{0,1,2\}$ is used to identify the IGBT i state in the leg k of the three-level converter, determining the switching function of each IGBT. The switching variables [13] are given by

$$n_k = \begin{cases} 2, & (S_{3k} \, e \, S_{4k}) = 1 \, e \, (S_{1k} \, e \, S_{2k}) = 0 \\ 1, & (S_{2k} \, e \, S_{3k}) = 1 \, e \, (S_{1k} \, e \, S_{4k}) = 0 \\ 0, & (S_{1k} \, e \, S_{2k}) = 1 \, e \, (S_{3k} \, e \, S_{4k}) = 0 \end{cases} \tag{14}$$

The level variable δ_{jn_k} with $j \in \{1,2\}$ is used to establish the charging state of the capacitor banks [13] and is given by

$$\delta_{jn_k} = \begin{cases} 0 & j > n_k \\ 1 & j \le n_k \end{cases} \tag{15}$$

The rectifier output voltage is given by

$$u_{sk} = \frac{1}{3}\sum_{j=1}^{2}(2\delta_{jn_k} - \sum_{\substack{l=1 \\ l \neq k}}^{3}\delta_{jn_l})U_{CRj} \quad k \in \{1,2,3\} \quad (16)$$

The DC voltage at the first set of capacity banks U_{dcRj}, i.e., at the rectifier side, is given by

$$\frac{dU_{dcR}}{dt} = \sum_{j=1}^{2}\frac{1}{C_{Rj} + C_{dc}}i_{CRj} \quad (17)$$

The linking between the first set of two capacity banks on offshore to a second one on onshore is assumed to be by a high voltage DC transmission submarine cable. The submarine cable is modeled by a π equivalent circuit model [11]. The current i_{dc} in the submarine cable is given by

$$\frac{di_{dc}}{dt} = \frac{1}{L_{dc}}(U_{dcR} - U_{dcI} - R_{dc}i_{dc}) \quad (18)$$

The DC voltage at the second set of capacity banks U_{dcIj}, i.e., at the inverter side, is given by

$$\frac{dU_{dcI}}{dt} = \sum_{j=1}^{2}\frac{1}{C_{Ij} + C_{dc}}i_{CIj} \quad (19)$$

The inverter input voltage is given by

$$u_{sk} = \frac{1}{3}\sum_{j=1}^{2}(2\delta_{jn_k} - \sum_{\substack{l=4 \\ l \neq k}}^{6}\delta_{jn_l})U_{CIj} \quad k \in \{4,5,6\} \quad (20)$$

E. Electric Network

The electric network is modeled by an equivalent three-phase active symmetrical circuit given by a series of a resistance and an inductance. So, the electric current injected, into the electric network is given by

$$\frac{di_{fk}}{dt} = \frac{1}{L_n}(u_{fk} - R_n i_{fk} - u_k) \quad k = \{4,5,6\} \quad (21)$$

This model for the electric network is usually used in transient studies and corresponds to what is said to be an infinite grid model linked by the equivalent series impedance.

III. CONTROL STRATEGY

A classical PI controller is used to acquire current references. IGBTs on/off switching states imply that the three-level converter is a time variant system. Therefore the SM control strategy is crucial for the operation of the three-level converter, assuring the assortment of the proper space vectors. Additionally, PWM by SVM, associated with SM, are used for triggering the IGBTs. The SM strategy's aim is to let the system slide along a predefined dynamic, also known as sliding surface, $A(e_{\alpha\beta},t)$, by changing the system structure, i.e., by changing the IGBTs on/off state. The IGBTs can only switch at finite frequency, due to physical limitations causing the control current not to be able to follow exactly the reference current, thus incurring in an error $e_{\alpha\beta}$. So, to maintain the system within the neighboring of the sliding surface, the state trajectory must comply with the conditions [13] given by

$$A(e_{\alpha\beta},t) \; dA(e_{\alpha\beta},t)/dt < 0 \quad (22)$$

A small error is acceptable in practice and a convenient achievement of this strategy is accomplished with hysteresis comparators [13]. If the current error, given by the comparators hysteresis output, $\sigma_{\alpha\beta}$, is quantified in five levels is possible to relate the space vectors with the current error. So $\sigma_{\alpha\beta}$ are integers numbers taking the values in the set $\{-2,-1,0,1,2\}$.

The output vectors for level 0, level 1 and level 2 in the $\alpha\beta$ plane for the three-level converter are shown in Fig. 4.
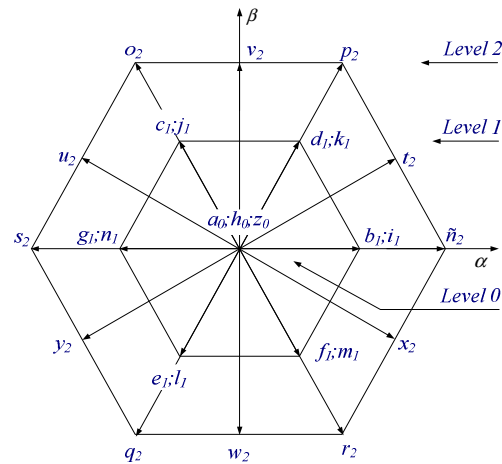

Fig. 4. Three-level converter, space vectors.

Some of the vectors are redundant ones, corresponding to different voltage level selection. The control strategy carries out a reduction on the capacitors banks unbalancing voltage by considering three vector tables, which take in account the voltage level of each capacitor bank in order to define the vector to use. Table I, II and III summarizes the vector selection for level 0, level 1 and level 2, respectively.

TABLE I. SPACE VECTOR SELECTION FOR LEVEL 0

$\sigma_\beta \setminus \sigma_\alpha$	-2	-1	0	1	2
-2	q_2	q_2	w_2	r_2	r_2
-1	y_2	e_1	e_1	x_2	x_2
0	s_2	g_1	a_0	b_1	$\tilde{n}_2$
1	u_2	c_1	c_1	t_2	t_2
2	o_2	o_2	v_2	p_2	p_2

TABLE II. SPACE VECTOR SELECTION FOR LEVEL 1

$\sigma_\beta \setminus \sigma_\alpha$	-2	-1	0	1	2
-2	q_2	q_2	w_2	r_2	r_2
-1	y_2	l_1	f_1	f_1	x_2
0	s_2	g_1	h_0	i_1	$\tilde{n}_2$
1	u_2	j_1	d_1	d_1	t_2
2	o_2	o_2	v_2	p_2	p_2

TABLE III. SPACE VECTOR SELECTION FOR LEVEL 2

$\sigma_\beta \setminus \sigma_\alpha$	-2	-1	0	1	2
-2	q_2	q_2	w_2	r_2	r_2
-1	y_2	y_2	m_1	m_1	x_2
0	s_2	n_1	z_0	i_1	$\tilde{n}_2$
1	u_2	u_2	k_1	k_1	t_2
2	o_2	o_2	v_2	p_2	p_2

IV. CASE STUDY

The offshore wind system has a nominal power of 2 MW. The mathematical model for the offshore wind system with the three-level is implemented in Matlab/Simulink. The wind speed considered in the simulation has a profile, see Fig. 5, having an average speed starting with a value of 10 m/s followed by a ramp increase stabilizing after 1.5 s with a speed of the 20 m/s, i.e., after 1.5 s the wind average speed is constant. The significant wave height and the frequency are respectively 10 m and 0.25 Hz. The electric network has 1 kV at 50 Hz. The case study is intended to assess the consequences of a malfunction on the rectifier input voltage at one phase assumed to impose $v_{s3} = 0$ V and occurring between 2.45 s and 2.80 s. So, the malfunction occurs when the wind is with a constant average speed.

The wind speed considered used in the simulation has a profile modeled by (1) and is shown in Fig. 5.
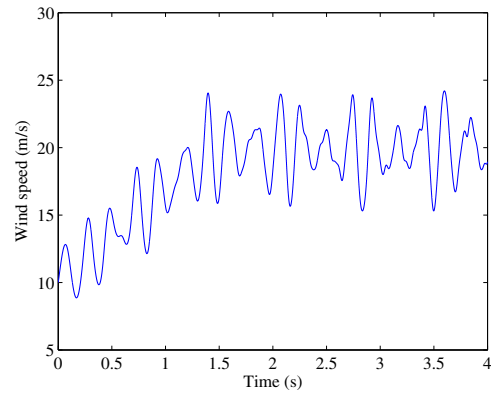

Fig. 5. Wind speed profile.

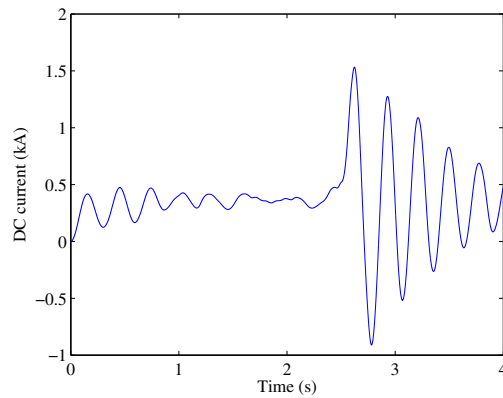The DC current at the submarine cable is shown in Fig. 6.

Fig. 6. DC current at the submarine cable.

The results for the DC voltage and the reference voltage on the capacitor banks at the rectifier side are shown in Fig. 7.
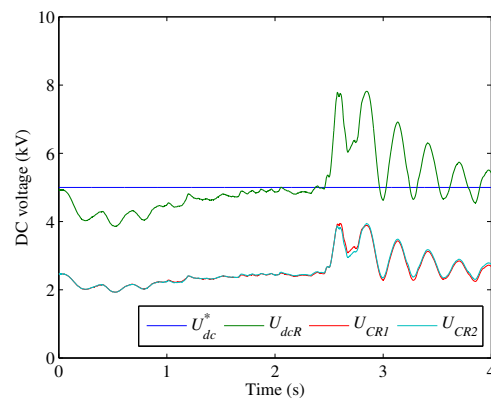

Fig. 7. DC voltages at the capacitor banks, rectifier side.

The results for the DC voltage and the reference voltage on the capacitor banks at the inverter side are shown in Fig. 8.
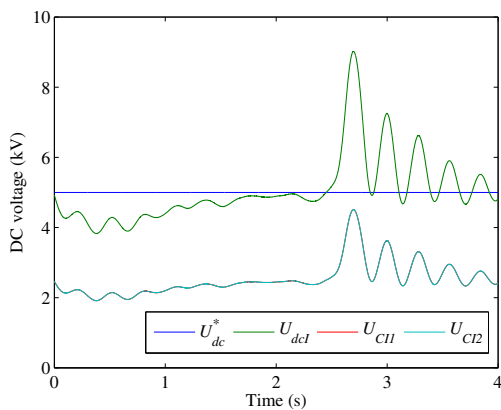

Fig. 8. DC voltages at the capacitor banks, inverter side.

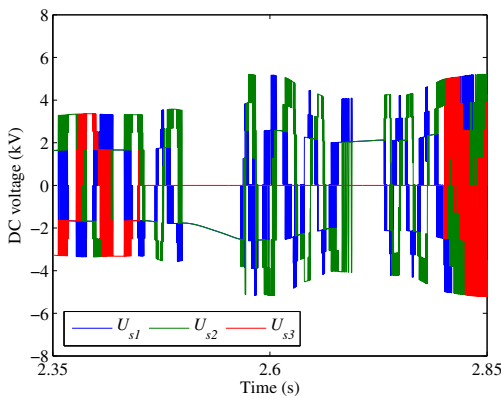The rectifier input voltage malfunction at one phase is shown in Fig. 9.

Fig. 9.   Rectifier input voltage malfunction.

V. CONCLUSIONS

The growing interest in the offshore wind turbine deployment requires further research of better mathematical models for offshore wind systems, allowing an improved capability to decide convenient measures. A modeling for an offshore wind systems linked to the electric network is proposed. The wind system is equipped with three-level converters topology in a rectifier and an inverter linked through a HVDC submarine cable. The wind turbine drive train is model by discrete three masses: the first is associated with the inertia of the blades flexible part; the second, with the blades rigid part, hub, tower and platform, discarding the movement between the different elements, but including the floating motion influence as an whole on the second; the third mass, with the rotor of the generator. The usefulness of the proposed method is illustrated by a study of a rectifier malfunction at one phase. The simulation of the malfunction allows concluding that the system is capable of having an adequate performance, despite the severe wind profile and wave height, i.e., restores the correct operation after the malfunction. But, eventually measures have to be taken to avoid outages on components of the system. For instances, although a during short time period, the DC current at the submarine cable and the capacitor banks voltage suffer a perturbation. So, assessment at the level of design on safety should be further carried out in function of the level of the current and of the voltage to be sustained during the short period by those components of the system. Also, the case study allows concluding that the control strategy carries out a reduction on the capacitors banks unbalancing voltage, either on the rectifier side or on the inverter side, i.e., the control keeps an appropriated behavior during the malfunction.

References

[1] M. Tao, Y. Hongxing , L. Lin, "A feasibility study of a stand-alone hybrid solar–wind–battery system for a remote island, " Applied Energy, vol. 121, pp 149–158, May 2014.

[2] T.F. Ishugaha, Y. Li, R.Z. Wang, J.K. Kiplagat, "Advances in wind energy resource exploitation in urban environment: A review," Renewable and Sustainable Energy Reviews, vol. 37, pp 613-626, September 2014.

[3] R. Sarrias-Mena, L.M. Fernández-Ramírez,C.A. García-Vázquez,F. Jurado, "Improving grid integration of wind turbines by using secondary batteries," Renewable and Sustainable Energy Reviews, vol 34, pp 194-207, June 2014.

[4] R. McKenna, S. Hollnaicher, W. Fichtner, "Cost-potential curves for onshore wind energy: A high-resolution analysis for Germany," Applied Energy vol 115, pp 103-115, February 2014.

[5] T. Soukissian, "Use of multi-parameter distributions for offshore wind speed modeling: the Johnson S_B distribution," Applied Energy vol 111, pp 982-1000, November 2013.

[6] B. Lange, S. Larsen, J. Højstrup, R. Barthelmie, "Importance of thermal effects and sea surface roughness for offshore wind resource assessment," Journal of Wind Engineering and Industrial Aerodynamics, vol 92, pp 959-988, September 2004.

[7] S. Xiaojing, H. Diangui, W. Guoqing, "The current state of offshore wind energy technology development," Energy, vol 41, pp 298-312, May 2012

[8] M.P. Gil, O. Gomis-Bellmunt, A. Sumper, and J. Bergas-Jané, "Power generation efficiency analysis of offshore wind farms connected to a SLPC (single large power converter) operated with variable frequencies considering wake effects," Energy, vol. 37, pp. 455 468, January 2012.

[9] V. Akhmatov, H. Knudsen, and A.H. Nielsen, "Advanced simulation of windmills in the electric power supply," Int. J. Electr. Power Energy Systems, vol. 22, pp. 421–434, 2000.

[10] J.G. Slootweg, H. Polinder, and W.L. Kling, "General model for representing variable speed wind turbines in power system dynamics simulations," IEEE Trans. P. S., vol. 18, pp. 144–151, February 2003.

[11] C. –M. Ong, Dynamic Simulation of Electric Machinery: Using Matlab/Simulink, New Jersey: Prentice-Hall, 1998, pp.259–350.

[12] T. Senjyu, S. Tamaki, N. Urasaki, and K. Uezato, "Wind velocity and position sensorless operation for PMSG wind generator," in Proc. 5th Int. Conf. on Power Electronics and Drive Systems 2003, Singapore, pp. 787–792.

[13] M. Seixas, R. Melício, and V.M.F. Mendes, "Fifth harmonic and sag impact on PMSG wind turbines with a balancing new strategy for capacitor voltages," Energy Conversion and Management, vol. 79, pp. 721–730, March 2014.